

OPEN

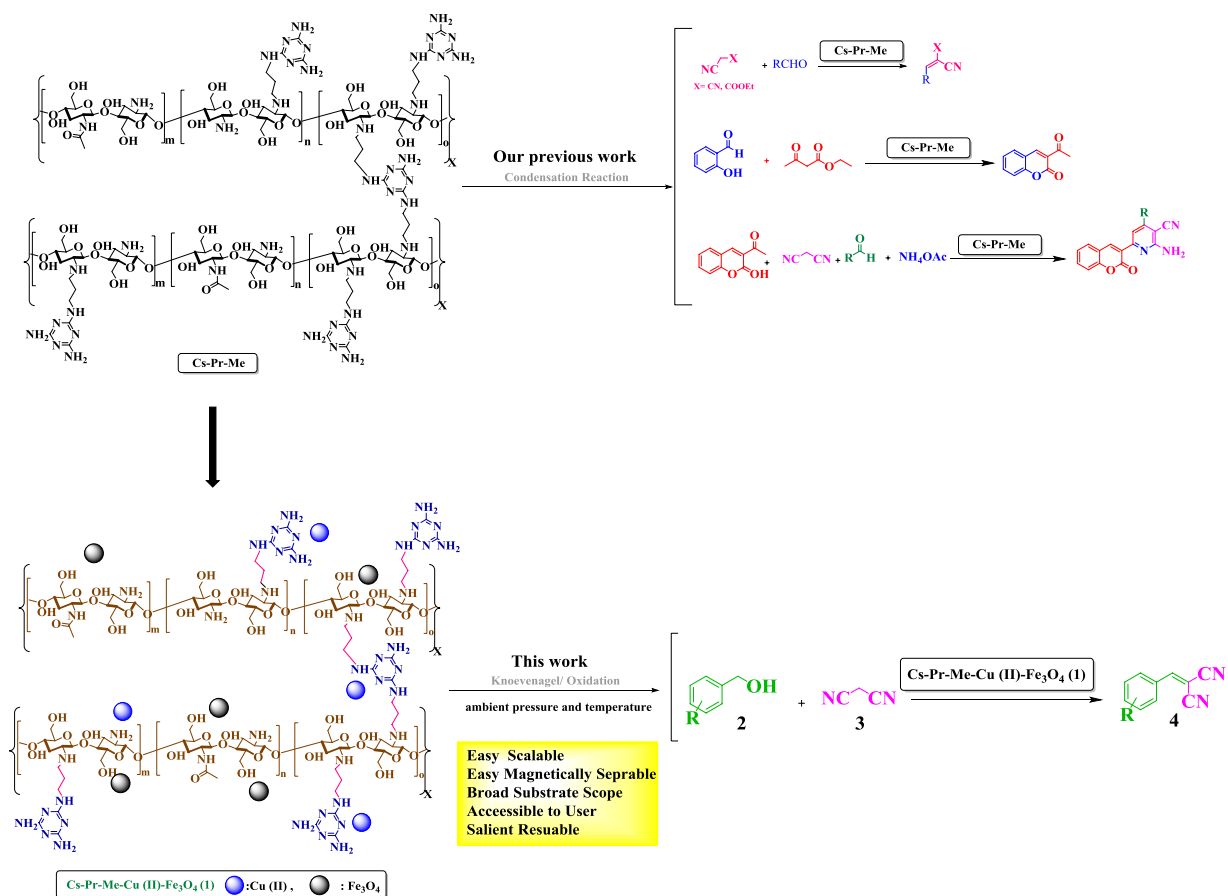
Cu(II) and magnetite nanoparticles decorated melamine-functionalized chitosan: A synergistic multifunctional catalyst for sustainable cascade oxidation of benzyl alcohols/Knoevenagel condensation

Zahra Alirezvani, Mohammad G. Dekamin* & Ehsan Valiey

The uniform decoration of Cu(II) species and magnetic nanoparticles on the melamine-functionalized chitosan afforded a new supramolecular biopolymeric nanocomposite (Cs-Pr-Me-Cu(II)-Fe₃O₄). The morphology, structure, and catalytic activity of the Cs-Pr-Me-Cu(II)-Fe₃O₄ nanocomposite have been systematically investigated. It was found that Cs-Pr-Me-Cu(II)-Fe₃O₄ nanocomposite can smoothly promote environmentally benign oxidation of different benzyl alcohol derivatives by *tert*-butyl hydroperoxide (TBHP) to their corresponding benzaldehydes and subsequent Knoevenagel condensation with malononitrile, as a multifunctional catalyst. Interestingly, Fe₃O₄ nanoparticles enhance the catalytic activity of Cu(II) species. The corresponding benzylidenemalononitriles were formed in high to excellent yields at ambient pressure and temperature. The heterogeneous Cs-Pr-Me-Cu(II)-Fe₃O₄ catalyst was also very stable with almost no leaching of the Cu(II) species into the reaction medium and could be easily recovered by an external magnet. The recycled Cs-Pr-Me-Cu(II)-Fe₃O₄ was reused at least four times with slight loss of its activity. This is a successful example of the combination of chemo- and bio-driven materials catalysis for mimicking biocatalysis as well as sustainable and one pot multistep synthesis.

Nanoparticles (NPs) have attracted great attention because of their unique optical, electrochemical, medical and catalytic properties^{1–8}. Indeed, the capacities and applications of NPs, as sorbent, sensor, heterogeneous catalyst, etc, are limited due to their low sustainability and dispersibility^{9–11}, deactivation or constant leaching, and low recyclability¹². Fortunately, the properties of NPs are affected seriously by support materials such as inorganic porous materials mainly silica or alumina¹³, organic polymers or biopolymers^{14,15}, dendrimers¹⁶, carbon nanotubes¹⁷, graphene oxide¹⁸, etc., which are essential for their applications specially in heterogeneous catalysis^{19–21}. Because of natural abundance, low toxicity compared to other transition metals and redox potential, copper is an appropriate metal used in nature for many oxidation reactions^{22–24}. Therefore, the immobilization of Cu(II) and magnetite NPs on multifunctional group supports can be considered as a feasible way to address above mentioned problems and sustainable chemistry principles^{11,25}. In this way, supramolecular chelation of Cu(II) species onto the surface of bifunctional modified chitosan with enhanced catalytic activity would be very desirable. This is a successful example of the combination of chemo- and bio-driven materials catalysis for mimicking biocatalysis as well as sustainable and one pot multistep synthesis^{26–32}. Indeed, one-pot multistep reactions which are also known as cascade reactions, do not require the isolation of intermediates and reduce the solvent wastes. Hence,

Pharmaceutical and Heterocyclic Compounds Research Laboratory, Department of Chemistry, Iran University of Science and Technology, Tehran, 1684613114, Iran. *email: mdekamin@iust.ac.ir



Scheme 1. Oxidation/Knoevenagel condensation of different benzyl alcohol derivatives with malononitrile in the presence of the Cs-Pr-Me-Cu(II)-Fe₃O₄ (1).

cascade reactions have attracted a great deal of attention in both academia and industry in recent decades^{29,33–36}. These reactions afford desired products in high to excellent yields and hence properly address green and sustainable chemistry principles. To date, most of the reported catalysts for one-pot cascade reactions are homogeneous, which typically suffer from product pollution and poor recyclability. Therefore, designing and introducing multifunctional catalysts with different catalytically active sites for one-pot cascade reactions is still a serious challenge.

Cyanocinamonitriles, which are prepared by the Knoevenagel condensation of a carbonyl group and C–H acids, serve as key intermediates in the synthesis of many important fine chemicals^{37–42}. Nowadays, the tandem oxidation of alcohols and Knoevenagel condensation reaction of the obtained aldehydes and active methylene compounds, as an economic and eco-friendly procedure towards cyanocinamonitriles, has also received a great attention from green and sustainable stand points of view^{35,43–47}. Traditionally, stoichiometric amounts of oxidants such as permanganates⁴⁸, chromium reagents⁴⁹ or the Dess-Martin periodinane⁴⁰ have been used for oxidation reactions with significant environmental impacts due to their toxicity and producing large amounts of waste. To address the aforementioned concerns, we were interested to modify chitosan, as a naturally abundant biopolymer with suitable ligands to afford multiple active sites⁵⁰. In the previous reports, we succeeded in covalently modification of chitosan with melamine and exploring of the activity of obtained Cs-Pr-Me as a bifunctional bio-derived organocatalyst^{51,52}. To our delight, the Cs-Pr-Me materials, with plentiful amino and hydroxyl groups in a proper geometry, was found to be a suitable support for the immobilization of Cu(II) and magnetic nanoparticles. Due to the economic and sustainable benefits of magnetic copper-based catalysts²⁵ and in continuation of our ongoing efforts towards developing efficient and novel heterogeneous catalysts^{15,51–56}, we wish herein to report preparation and characterization of the supramolecular Cu(II) and magnetite nanoparticles decorated melamine-functionalized chitosan (Cs-Pr-Me-Cu(II)-Fe₃O₄), as a recyclable catalyst, for green cascade oxidation/Knoevenagel condensation. Furthermore, the use of TBHP, as a green oxidant, is a reasonable choice⁵⁵ (Scheme 1).

Results and Discussion

The Cs-Pr-Me materials were prepared by grafting of melamine to the chitosan backbone using 1,3-dibromopropene, as an appropriate linker, according to our published procedures^{51,52}. In the next step, immobilization of the Cu(II) species on the Cs-Pr-Me backbone was achieved using an aqueous solution of Cu(OAc)₂. Then, the surface of Cs-Pr-Me were decorated *in situ* by magnetite nanoparticles. The obtained Cs-Pr-Me-Cu(II)-Fe₃O₄ materials were characterized in details with various analysis techniques and methods

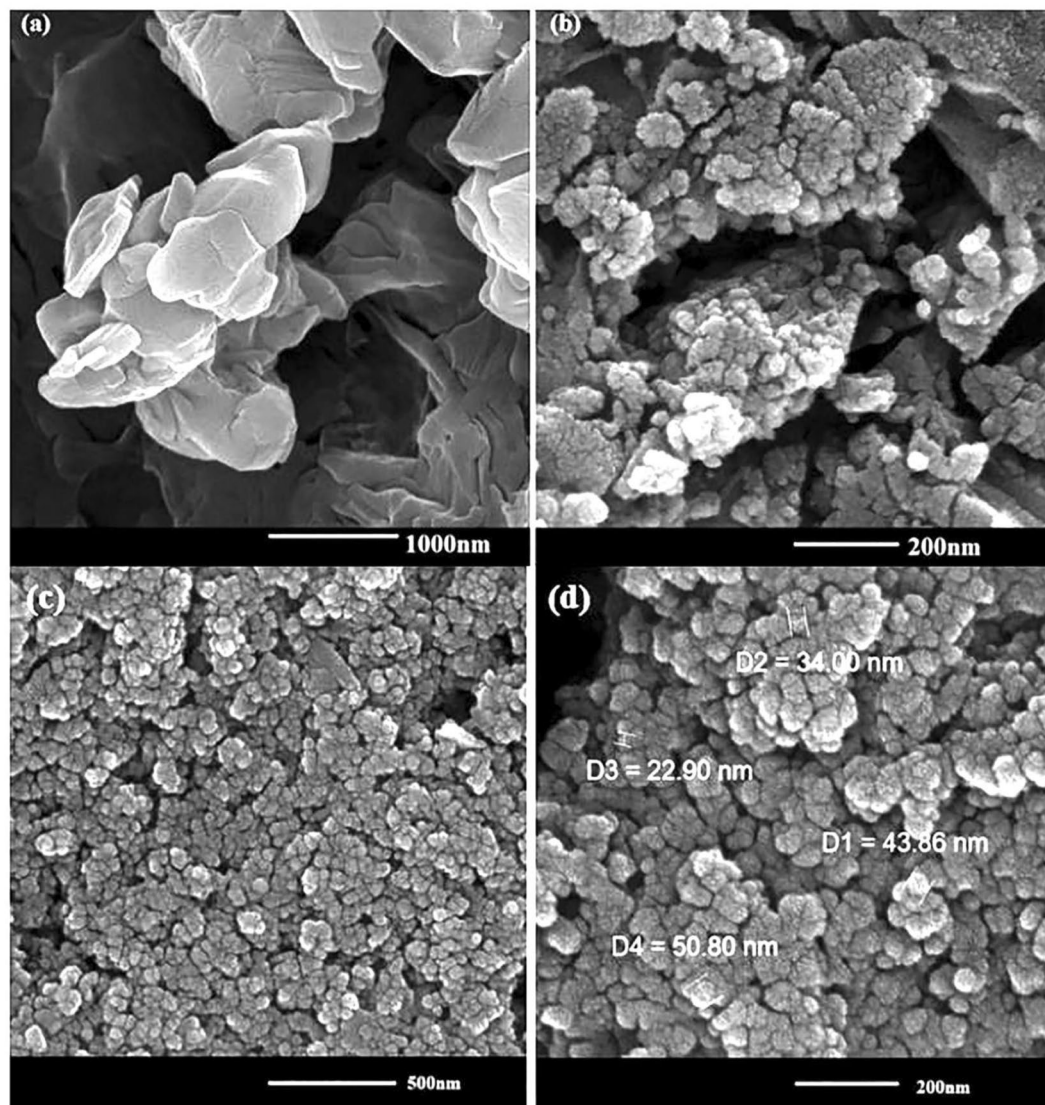


Figure 1. FESEM images of the commercial chitosan (a), Cs-Pr-Me materials before modification (b), and Cs-Pr-Me-Cu(II)-Fe₃O₄ (1) materials at 500 (c) and 200 nm (d) scales.

such as Fourier transform infrared (FTIR) spectroscopy, field emission scanning electron microscopy (FESEM), transmission electron microscopy (TEM), inductively coupled plasma (ICP), X-ray diffraction (XRD), energy dispersive X-ray (EDX) mapping analysis, and vibrating sample magnetometer (VSM).

The FTIR spectra of Cs-Pr-Me-Cu(II)-Fe₃O₄ (1) demonstrated the evidence for existence of Cu(II) and magnetite nanoparticles on the melamine-functionalized chitosan backbone. Fig. S1 illustrates the FTIR spectra of Cs-Pr-Me (a), fresh Cs-Pr-Me-Cu(II)-Fe₃O₄ (1, b) and Cs-Pr-Me-Cu(II)-Fe₃O₄ after four times recycling (1, c), respectively (See Electronic Supplementary Information). As shown in Fig. S1a, the Cs-Pr-Me showed the adsorption bands at 3567, 3453, 3450–3100 and 1390 cm⁻¹, which are attributed to the asymmetric and symmetric stretching vibrations of N–H bonds and the stretching vibration of O–H bonds of chitosan. Furthermore, the signals at 1616 and 1593 cm⁻¹ are assigned to the NH₂ and NCN bending vibrations of melamine. The OH bending vibration of chitosan corresponds to the broad signal in the range of 1470–1330 cm⁻¹. After formation of Cs-Pr-Me-Cu(II)-Fe₃O₄ (1), the above band intensities were decreased as shown in Fig. S1b, which represent Cu(II) and magnetite nanoparticles have been coordinated by the amino and hydroxyl functional groups of the Cs-Pr-Me materials. In addition, the characteristic bands for Fe–O and Cu–O stretching vibrations were observed at 560 and 430 cm⁻¹, respectively.

The morphological features and size of Cu(II) and magnetic iron oxide NPs were examined by FESEM and TEM experiments (Figs. 1 and 2). The FESEM images of the commercial chitosan and Cs-Pr-Me before modification have been shown in Fig. 1a,b, respectively. Furthermore, Fig. 1c,d show the FESEM images of Cs-Pr-Me-Cu(II)-Fe₃O₄ (1) materials. The Cu(II) and Fe₃O₄ nanoparticles are approximately spherical and scattered with an average diameter of about 23–51 nm. On the other hand, TEM images (Fig. 2) obviously demonstrate almost uniform decoration of Cu(II) species and magnetic nanoparticles on the melamine-functionalized chitosan support. Also, according to ICP analysis, the percentage of chelated copper and iron in the fresh

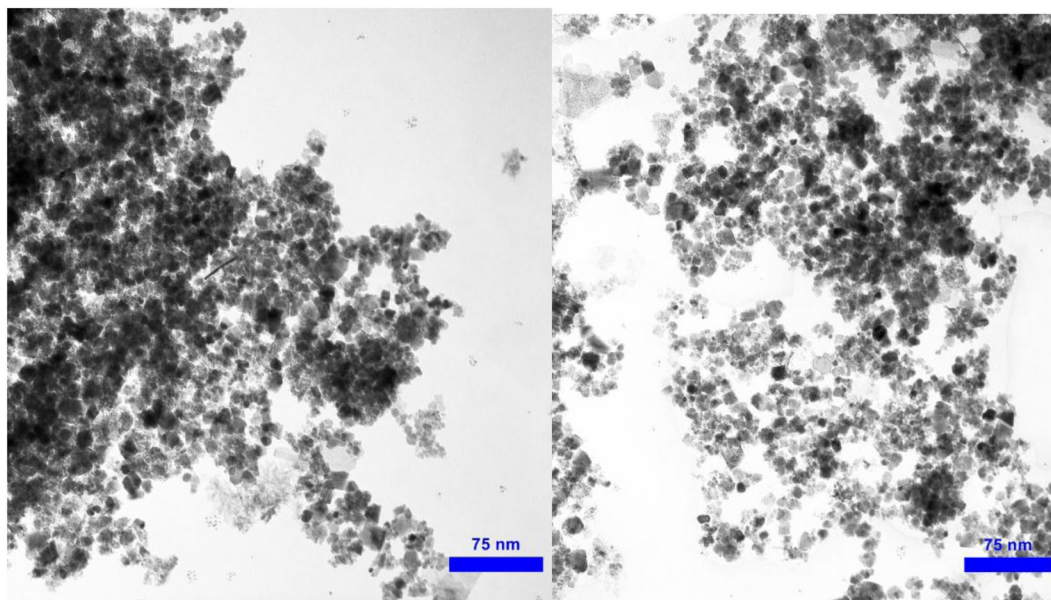


Figure 2. TEM images of the Cs-Pr-Me-Cu(II)-Fe₃O₄ (**1**) nanomaterials.

Cs-Pr-Me-Cu(II)-Fe₃O₄ (**1**) was found to be 1.38 wt% (Cu) and 25.72 wt% (Fe), respectively. The EDX spectrum of the Cs-Pr-Me-Cu(II)-Fe₃O₄ (**1**) is shown in Fig. 3. The EDX spectrum indicates that the introduced catalyst **1** materials are composed of Cu, Fe, O, N and C elements. In addition, EDX mapping was performed to observe distributions of the elements in the Cs-Pr-Me-Cu(II)-Fe₃O₄ (**1**) nanocomposite. As it can be seen in Fig. 3, the indicated elements, especially Cu and Fe, demonstrate uniform distributions. These obtained data strongly confirm successful immobilization of the Cu(II) species and iron oxide nanoparticles on the Cs-Pr-Me backbone. On the other hand, the magnetic properties of the Cs-Pr-Me-Cu(II)-Fe₃O₄ (**1**) was measured using vibrating sample magnetometer (VSM) at room temperature. As it was seen in Fig. S5, the value of the saturation magnetization was 67 emu/g for the Cu(II) species and magnetic nanoparticles decorated melamine-functionalized chitosan (**1**, See Electronic Supplementary Information).

Also, Fig. 4 shows the XRD patterns of the fresh Cs-Pr-Me-Cu(II)-Fe₃O₄ (**1**) materials and the recycled sample. The XRD patterns of the melamine and chitosan are also illustrated for comparison as offset patterns. The diffraction peaks at 2θ values of 43.30, 50.40 and 74.15° can be attributed to the reflections of cubic Cu (JCPDS No. 04-0836, marked with ●). Moreover, the peaks at 2θ values of 30.20, 35.39, 36.89, 53.31, 56.98, 73.91° can be assigned to the reflections of cubic Fe₃O₄ (JCPDS No. 019-0629, marked with ▲). On the other hand, the well-defined high intensity diffraction signals (2θ) at 13.41, 17.95, 21.65, 22.25, 26.28, 28.90 and 29.91° are in accordance with the monoclinic crystal system of melamine (JCPDS no. 024-1654). Furthermore, the lower intensity for the diffraction peaks of Cu and Fe₃O₄ may be due to their lower weights compared to that of Cs-Pr-Me support in the structure of nanocomposite **1**.

Cs-Pr-Me-Cu(II)-Fe₃O₄ nanomaterials-promoted cascade oxidation/Knoevenagel condensation for the synthesis of α,β -unsaturated nitriles **4a-f.** To evaluate the catalytic activity of Cs-Pr-Me-Cu(II)-Fe₃O₄ (**1**), the one-pot oxidation/Knoevenagel condensation between benzyl alcohol (**2a**) and malononitrile (**3**) in CH₃CN was chosen as the model reaction. As the information in Table 1 show, in the absence of the catalyst **1** and using different oxidants including TBHP, H₂O₂, O₂, and air, no condensation product, 2-benzylidinemalononitrile (**4a**), was formed at 80 °C. However, 58%, 75% and 20% conversion to benzoic acid **6a** was observed when TBHP, H₂O₂, and O₂ were used, respectively. On the other hand, only trace amounts of bezaldehyde **5a** and benzoic acid **6a** were formed when the reaction mixture was subjected to an air flow (Table 1, entries 1–4). Interestingly, 23% of the desired benzylidinemalononitrile **4a** was observed by employing 10 mg of Cs-Pr-Me-Cu(II)-Fe₃O₄ (**1**), as a catalyst, without any oxidant (Table 1, entry 5). Among TBHP and H₂O₂, the former was found to be more effective for the reaction (Table 1, entries 6–7). Indeed, H₂O₂ afforded lower yeild of the desired product **4a** compared to TBHP. In fact, the hydroxyl radical produced by H₂O₂ is a more powerful oxidant compared to the *t*-BuOO radical generated by TBHP during the reaction. It has been reported before that the OH radical reacts with polysaccharides such as chitosan to depolymerize them and forming chitosan chains with lower molecular weights⁵⁷. Therefore, the lower yeild of the desired product **4a** can be attributed to the higher tendency of OH radicals to depolymerize the chitosan cahins in the structure of the catalyst **1** rather than oxidation of benzyl alcohol (Table 1, entry 7). Hence, TBHP was used in the next optimization experiments. To our delight, by reducing the reaction tempereture, the desired product **4a** was formed in the same yeilds at 60 °C and room temperature, however longer times were required (entries 8,9). Hence, room temperature was chosen as a sustainable conditions for the reaction although it requires a longer time. Furthermore, the nature of the solvent showed a significant impact on the oxidation of benzyl alcohol (**2a**) and subsequent Knoevenagel condensation. For instance, toluene and H₂O afforded the desired product **4a** in lower yeilds compared to CH₃CN

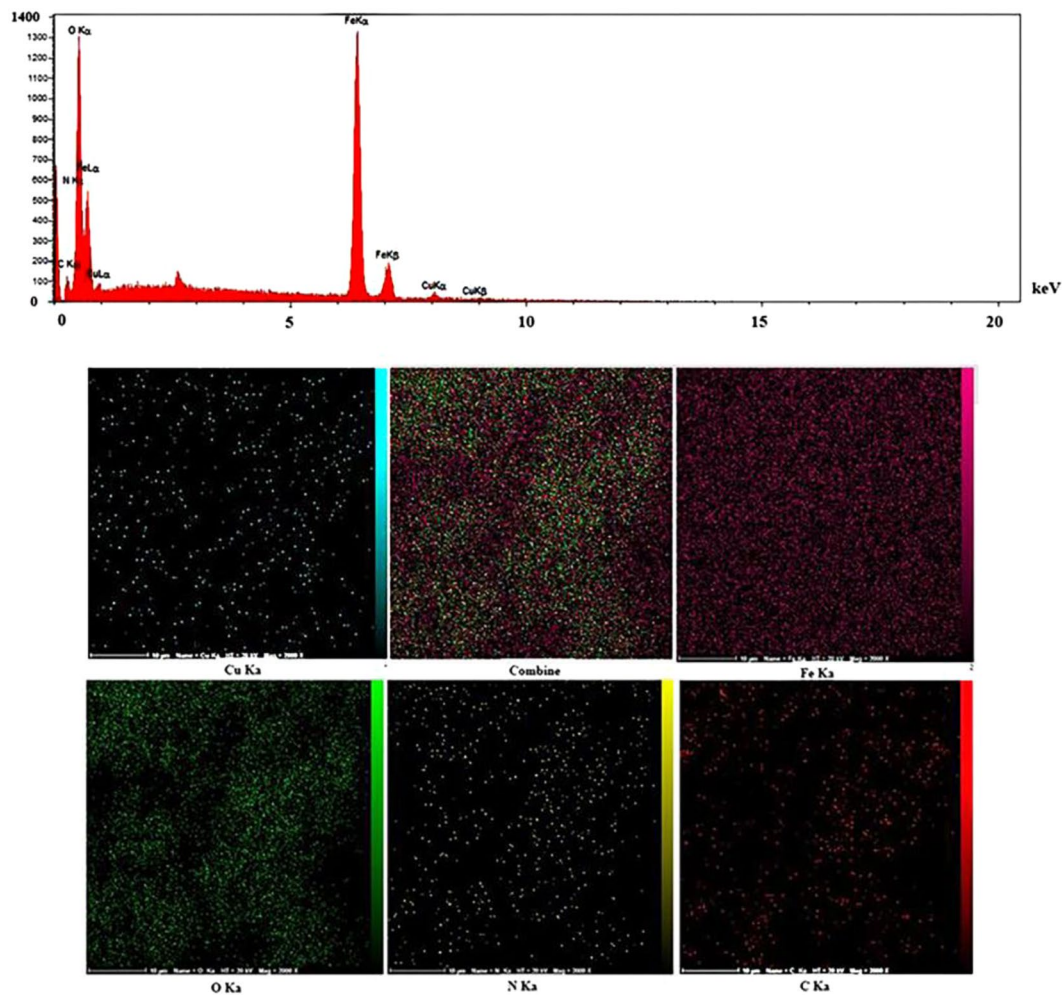


Figure 3. Energy dispersive spectroscopy (EDX) pattern and elemental mapping of the Cs-Pr-Me-Cu(II)-Fe₃O₄ (1) nanocomposite.

under the same catalyst loading even after longer times (Table 1, entries 10,11). Upon increasing of the catalyst loading from 5 to 20 mg, the conversion of benzyl alcohol **2a** to 2-benzylidene malononitrile (**4a**) considerably increased (Table 1, entries 7, 12–14). It is noteworthy that the Cs-Pr-Me-Cu(II) materials afforded a lower yield compared to the Cs-Pr-Me-Cu(II)-Fe₃O₄ (**1**) under the same conditions (entries 14, 15). This can be attributed to the involvement of Fe(III) species in the catalytic cycle (See Scheme 2).

In the next step, the effect of TBHP oxidant equivalent against benzyl alcohol (**2a**) was systematically investigated in 4 h intervals. The results have been shown in Fig. 5. The results of this part of our study showed that one equivalent of TBHP oxidant afforded the desired oxidation/Knoevenagel product **4a** with 100% conversion after 8 h. On the other hand, higher or lower equivalents of TBHP oxidant produced lower yields of the desired oxidation/Knoevenagel product **4a**. Encouraged by these results, the substrate scope of this oxidation/Knoevenagel condensation was studied in the next step under the optimal conditions. Table 2 shows the summarized results.

As revealed in Table 2, the reaction conditions were compatible with both electron-withdrawing and electron-donating substituents at *p*- as well as *o*- positions of the aromatic ring. Interestingly, 2-benzylidene malononitrile (**2a**) could be obtained from corresponding substrate in 100% conversion. Furthermore, alcohols such as *p*-hydroxybenzyl alcohol (**2d**) and *p*-nitrobenzyl alcohol (**2e**), reacted slowly to form the corresponding aldehydes in good conversions. On the other hand, 2-pyridylmethanol (**2f**) did not afford oxidation/Knoevenagel condensation product **4f** under optimized reaction conditions. However, it was partially converted to its corresponding carboxylic acid **6f** when two or more equivalents of TBHP was used. This observations can be attributed to fast conversion of substrate **2f** to its corresponding *N*-oxide which rearrange subsequently to the corresponding 2-pyridinecarboxylic acid (**6f**)^{58,59}.

According to the above observations, a plausible free radical mechanism, as shown in Scheme 2, can be proposed for the cascade oxidation/Knoevenagel condensation of different benzyl alcohols **2** by TBHP in the presence of Cs-Pr-Me-Cu(II)-Fe₃O₄ (**1**). First, TBHP is broken down into *t*-butylperoxide radical and proton by reduction of Cu⁺² and Fe⁺³ ions. Abstraction of a hydrogen radical from benzyl alcohol derivatives **2** affords corresponding benzyl radicals (**I**) which can combine later with *t*-butylperoxide radical to form corresponding benzaldehydes (**II**). Next, the obtained aromatic aldehydes and malononitrile (**3**) are activated by the Lewis acidic and basic sites of multifunctional catalyst **1**, respectively via a typical Knoevenagel condensation route. Finally,

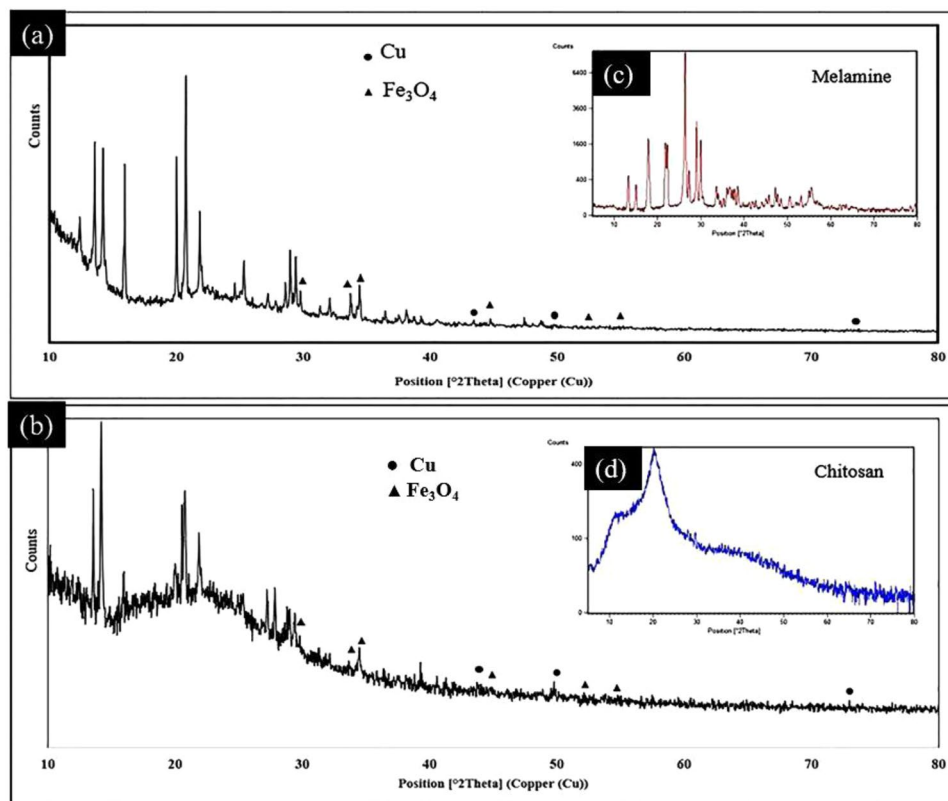
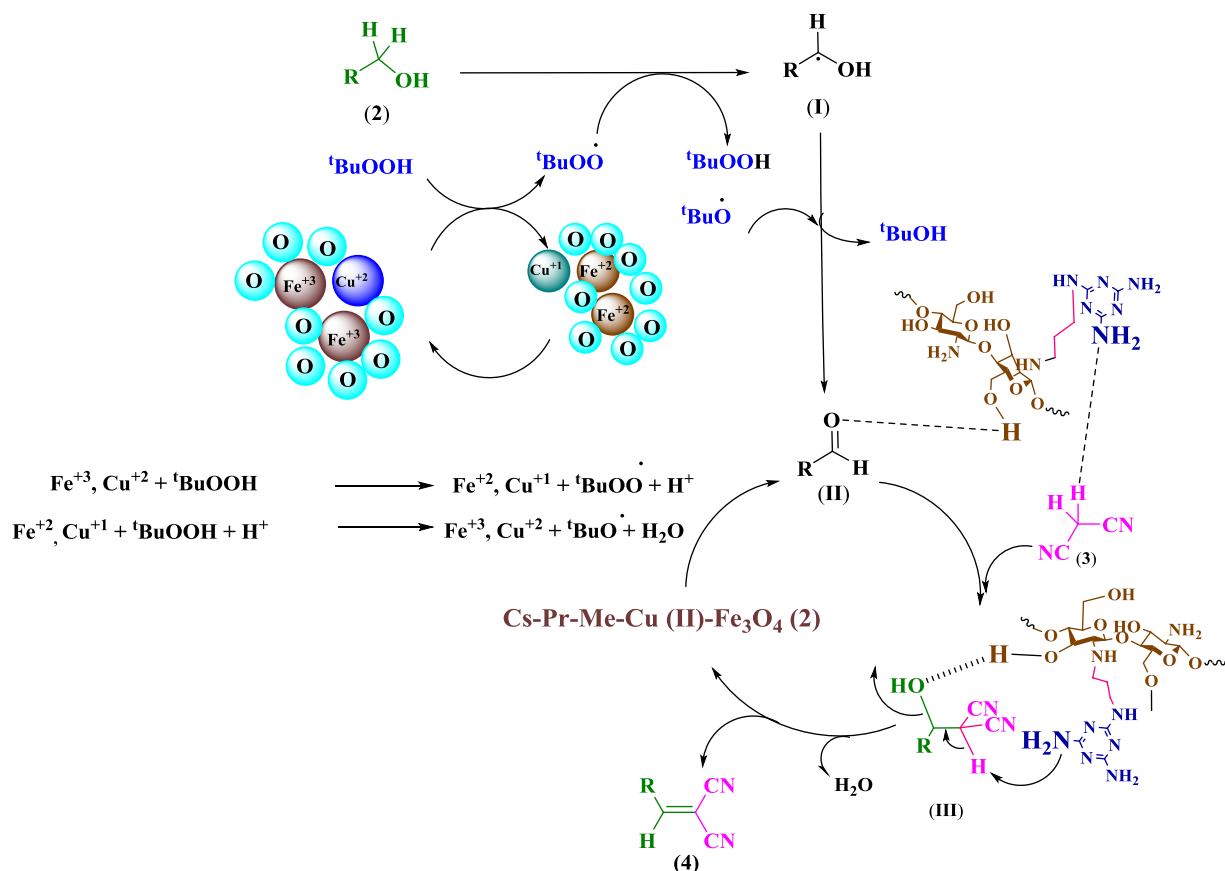


Figure 4. XRD patterns of the fresh Cs-Pr-Me-Cu(II)-Fe₃O₄ materials (1, a), recycled sample after five runs (b), melamine (c) and commercial chitosan (d).

Reaction scheme: Benzyl alcohol (2a) reacts with catalyst 3 (CH₃(CN)₂) and oxidant to form Knoevenagel condensation product (4a), benzaldehyde (5a), and benzoic acid (6a).

Entry	Catalyst	Catalyst loading (mg)	Oxidant	Solvent	Temperature (°C)	Time (h)	Conversion (%) 4a	Conversion (%) 5a	Conversion (%) 6a
1	—	—	TBHP ^b	CH ₃ CN	80	24	—	Trace	58
2	—	—	H ₂ O ₂	CH ₃ CN	80	24	—	Trace	75
3	—	—	O ₂	CH ₃ CN	80	24	Trace	Trace	20
4	—	—	Air	CH ₃ CN	80	24	—	Trace	Trace
5	Cs-Pr-Me-Cu(II)-Fe ₃ O ₄ (1)	10	—	CH ₃ CN	80	24	23	Trace	—
6	Cs-Pr-Me-Cu(II)-Fe ₃ O ₄ (1)	10	TBHP ^b	CH ₃ CN	80	6	64	—	—
7	Cs-Pr-Me-Cu(II)-Fe ₃ O ₄ (1)	10	H ₂ O ₂ ^b	CH ₃ CN	80	6	16	trace	27
8	Cs-Pr-Me-Cu(II)-Fe ₃ O ₄ (1)	10	TBHP ^b	CH ₃ CN	60	9	62	—	—
9	Cs-Pr-Me-Cu(II)-Fe ₃ O ₄ (1)	10	TBHP ^b	CH ₃ CN	r.t.	12	62	—	—
10	Cs-Pr-Me-Cu(II)-Fe ₃ O ₄ (1)	10	TBHP ^b	Toluene	r.t.	15	58	—	—
11	Cs-Pr-Me-Cu(II)-Fe ₃ O ₄ (1)	10	TBHP ^b	H ₂ O	r.t.	24	34	27	—
12	Cs-Pr-Me-Cu(II)-Fe ₃ O ₄ (1)	5	TBHP ^b	CH ₃ CN	r.t.	12	62	—	—
13	Cs-Pr-Me-Cu(II)-Fe ₃ O ₄ (1)	15	TBHP ^b	CH ₃ CN	r.t.	10	87	—	—
14	Cs-Pr-Me-Cu(II)-Fe ₃ O ₄ (1)	20	TBHP ^b	CH ₃ CN	r.t.	8	100	—	—
15	Cs-Pr-Me-Cu(II)	20	TBHP ^b	CH ₃ CN	r.t.	10	93	—	—

Table 1. Screening of different conditions on the oxidation/Knoevenagel condensation products of benzyl alcohol (2a)^a. ^aThe model reaction was run at 5 mmol scale. ^b5 mmol of TBHP or H₂O₂ was used for the reaction.



Scheme 2. Plausible mechanism for the oxidation/Knoevenagel condensation of different benzyl alcohols 2a-f catalyzed by Cs-Pr-Me-Cu(II)-Fe₃O₄ (1).

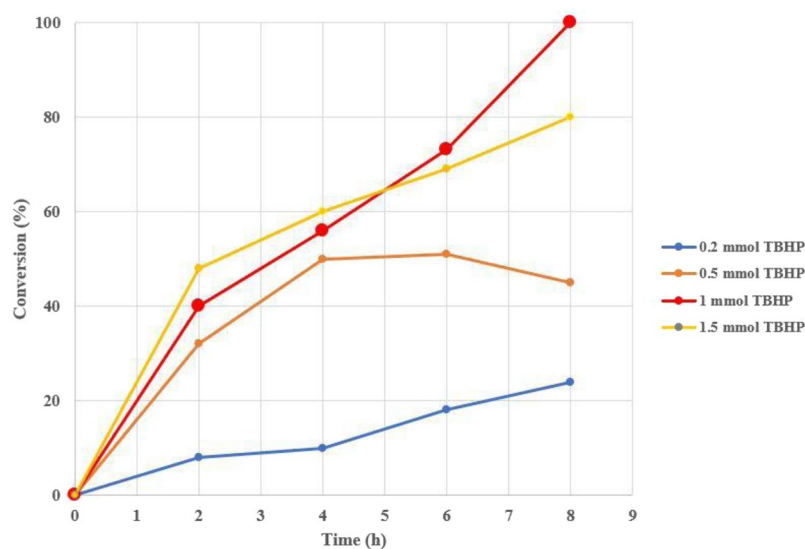


Figure 5. The effect of different TBHP oxidant: benzyl alcohol (2a) mole ratios on the yield of oxidation/Knoevenagel condensation product 4a.

elimination of one molecule of water affords desired products 4(a-f)^{60,61}. It should be noted that the hygroscopic nature of the chitosan backbone of the supramolecular catalyst 1 can additionally adsorb water molecules on its surface and hence promote smoothly the Knoevenagel condensation^{15,51,62}.

Furthermore, reusability of a heterogeneous catalyst is an important feature for its efficiency and future industrial application. Consequently, we studied the reusability of the Cs-Pr-Me-Cu(II)-Fe₃O₄ (1) up to fifth cycle

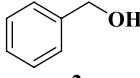
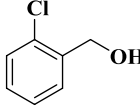
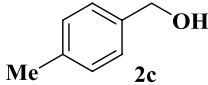
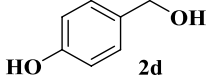
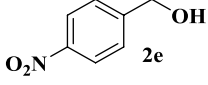
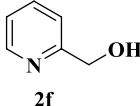
Entry	Substrate 2	Time (h)	Crude Yield (%)	Conversion (%)		
				4a-f	5a-f	6a-f
1	 2a	8	87	100	—	—
2	 2b	8	91	79	—	—
3	 2c	7	86	51	—	—
4	 2d	12	69	88	—	—
5	 2e	11	64	67	—	—
6	 2f	24 ^c	47	—	—	43
		24 ^d	95	—	—	90

Table 2. Scope of the cascade oxidation/Knoevenagel condensation of different benzyl alcohols **2a-f** catalyzed by Cs-Pr-Me-Cu(II)-Fe₃O₄ (**1**) under optimized conditions^{a,b}. ^aReaction conditions: benzyl alcohol derivatives (**2**, 1 mmol), malononitrile (**3**, 1.1 mmol) and the Cs-Pr-Me-Cu(II)-Fe₃O₄ (**1**, 20 mg) in CH₃CN at room temperature. ^bAll products are known and their structures and conversion were established from their ¹H NMR spectra data and melting points as compared with authentic samples or literature values. ^c1 mmol of TBHP was used. ^d2 mmol of TBHP was used.

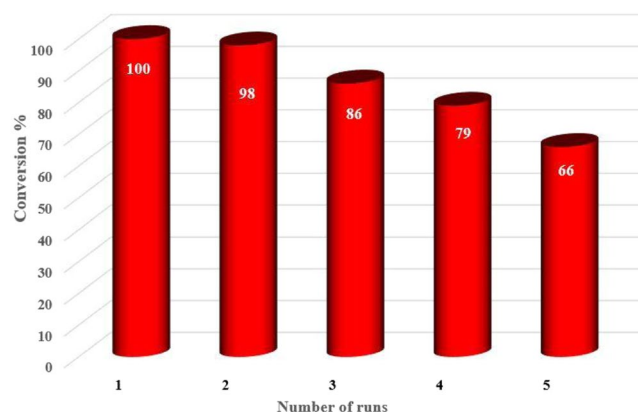


Figure 6. Reusability of the heterogeneous nanocatalyst Cs-Pr-Me-Cu(II)-Fe₃O₄ (**1**) for the synthesis of **4a**.

(Fig. 6). Therefore, the catalyst **1** was magnetically separated from the reaction mixture, washed with acetone and hexane to remove any organic impurities and dried in an oven. After drying, it was again used for oxidation/Knoevenagel condensation following the same procedure as mentioned in the experimental section. As data in Fig. 6 show, the decrease of catalytic activity of the nanocomposite **1** from the first run to the second run was slight (about 2%). However, more decrease (about 12%) was observed in the next runs with the recycled catalyst **1**. According to ICP analysis results, the percentage of copper and iron in the fresh Cs-Pr-Me-Cu(II)-Fe₃O₄ (**1**) was found to be 1.38 wt% (Cu) and 25.72 wt% (Fe), respectively. On the other hand, the percentage of copper and iron in the recycled Cs-Pr-Me-Cu(II)-Fe₃O₄ (**1**) after five runs was observed to be 1.26 wt% (Cu) and 25.16 wt% (Fe), respectively. This means that relative percentage of copper loss (8.8 wt%) in the recycled catalyst after five runs is higher than iron loss (2.2 wt%) compared to the fresh sample. These observations can be interpreted to more loss of melamine units, as a more probable chelating agent of Cu(II) species, compared to chitosan monomers with more tendency to chelate Fe₃O₄ nanoparticles. Indeed, some parts of the covalent bonds between melamine and chitosan may be broken during mechanical stirring and heating required for reaction or recycling. On the other hand, bridge methylene groups in the 1,3-propylene linker are more labile to be partially oxidised and

Entry	Catalyst	Catalyst loading	Oxidant	Temperature (°C)	Time (h)	Conversion (%)	Catalyst reuse times	References
1	Ru(OH) _x supported on polyethylenimine modified magnetic nanoparticles coated with silica	100 mg	O ₂	two steps (110 °C + r.t.)	2 steps (10 + 12)	99	2	64
2	NiGa Layered Double Hydroxide (CO ₃ ⁻² @Ni ₃ Ga-LDH)	50 mg	O ₂	80 °C	2 steps (4 + 2)	80	5	45
3	Gold nanoparticles deposited on an amino-functionalized Al-based MIL-53 metal-organic framework (Au@MIL-53(NH ₂))	1 mol%	O ₂	100 °C	13	99	5	44
4	RuCl ₃ on MOF UiO-66 (UiO-66-Ru)	3.6 mol % Ru	(3.6 mol % Ru)	100 °C	6	100	—	34
4	Cs-Pr-Me-Cu(II)-Fe ₃ O ₄ (1)	20 mg	TBHP	r.t	8	100	4	This work

Table 3. Comparison of the catalytic activity of Cs-Pr-Me-Cu(II)-Fe₃O₄ (1) with other reported catalysts for the synthesis of the 2-benzylidenemalononitrile (2a).

subsequently facilitate break down of the melamine units from the modified polymer backbone through hydrolysis during reaction, separation or recycling⁶³. On the other hand, Fig. 4(b) shows the XRD patterns of the recycled catalyst **1** after five runs used in the model reaction. As can be seen, there is very good coincident between the powder XRD signals of the fresh Cs-Pr-Me-Cu(II)-Fe₃O₄ (1) and the recycled sample.

To demonstrate the efficiency and merits of the Cs-Pr-Me-Cu(II)-Fe₃O₄ supramolecular catalyst (1) for the cascade oxidation/Knoevenagel condensation of different benzyl alcohols, it has been compared with some of the recently catalytic systems. The comparison has been summarized in Table 3. It is obvious that the present catalytic system requires low loading of a nontoxic and inexpensive transition metal species working at room temperature to afford one-pot oxidation/Knoevenagel condensation products in one step.

Experimental Section

General Information. All reagents and solvents were obtained from commercial suppliers and used without further purification. Chitosan (MW = 10000–30000 Da) was purchased from Acros Organics. ¹H NMR spectra were recorded at 500 MHz using a Bruker DRX-500 Avance spectrometers in DMSO-*d*₆ or CDCl₃ as the solvent. Characterization of the catalyst **1** was carried out using FESEM TESCAN-MIRA3, EDX Numerix DXP-X10P, VSM (BHV-55, Riken, Japan), Shimadzu FT-IR-8400S and TEM Philips CM30. The analytical thin layer chromatography (TLC) experiments were performed using Merck 0.2 mm silica gel 60 F-254 Al-plates.

General procedure for preparation of the Cs-Pr-Me-Cu(II)-Fe₃O₄ (1). The melamine-functionalized chitosan (Cs-Pr-Me) was first prepared according to the procedure described in our previous works^{51,52}. Next, the Cs-Pr-Me (1.0 g) was suspended in 50 mL of distilled water. To this suspension, Cu(OAc)₂ (0.5 g) was added and stirring was continued for 12 h. The final dispersed solution was centrifuged and the obtained solid was dried under vacuum for 1 h. Then, Fe₃O₄ nanoparticles were fabricated by *in-situ* coprecipitation as follows: Iron(III) chloride hexahydrate (4.6 g, 0.017 mol) and iron(II) chloride tetrahydrate (2.2 g, 0.011 mol) were dissolved in distilled water. The prepared Cs-Pr-Me-Cu(II) was then added into the obtained aqueous solution and heated to 50 °C under N₂ atmosphere. Then, 25% aqueous ammonia (10 mL) was slowly added to the obtained mixture under vigorous stirring. After 30 min, the precipitate was collected from the solution by an external magnet and washed three times with distilled water (3 × 5 mL). Finally, the obtained brown solid was dried in an oven at 60 °C for 2 h before using.

Typical procedure for the synthesis of α,β-unsaturated nitriles (4a-f) through cascade oxidation/Knoevenagel condensation catalyzed by the Cs-Pr-Me-Cu(II)-Fe₃O₄ (1). In a round-bottomed flask, benzyl alcohol (2, 1.0 mmol), TBHP (1.0 mmol) and Cs-Pr-Me-Cu(II)-Fe₃O₄ (1, 20 mg) were mixed in CH₃CN (2.0 mL) and stirred at room temperature. Then, malononitrile (3, 1.1 mmol) was added to the reaction mixture and the mixture was stirred for the appropriate times reported in Table 2. After completion of the reaction, the solvent was evaporated. Then, EtOAc (3 mL) was added to the mixture and the catalyst **1** was separated by an external magnet. Afterwards, n-hexane was added drop wise into the solution until benzylidenemalononitriles **4** were completely precipitated. The obtained mixture was filtered off and the precipitate were washed with n-hexane and then dried in an oven at 70 °C for 1 h. Alternatively, the products were extracted by EtOAc and the crude reaction mixture after evaporation of the solvent was analyzed by ¹H NMR (Figs. S6–S10, See Electronic Supplementary Information). The recycled catalyst **1** was washed with acetone and hexane (1 mL), respectively and then dried at 50 °C for 2 h and stored for another run.

Leaching test of the Cs-Pr-Me-Cu(II)-Fe₃O₄ (1). The Cs-Pr-Me-Cu(II)-Fe₃O₄ (1) was separated from the model reaction mixture after 4 h. The reaction was continued with the filtrate in the absence of nanocatalyst **1** for an extra 4 h. No further increase in the conversion of benzyl alcohol (2a) was observed, which approves the catalytically active sites for this oxidation/Knoevenagel condensation are located on the Cs-Pr-Me-Cu(II)-Fe₃O₄ (1) and do not disperse into the reaction mixture.

Conclusions

In summary, we have developed a cost-effective and practical route for fabrication of uniform Cs-Pr-Me-Cu(II)-Fe₃O₄ nanomaterials for the first time. The new Cs-Pr-Me-Cu(II)-Fe₃O₄ supramolecular catalyst was found to be, a valuable magnetically reusable catalyst for sustainable cascade oxidation/Knoevenagel condensation of benzyl alcohols to their corresponding α,β -unsaturated nitriles under truly mild reaction conditions. Significant advantages of the present work are as follows: high to quantitative conversion of benzyl alcohols, mild reaction conditions, scalable synthesis, simple separation of the catalyst using an external magnet and reusability of the catalyst for at least five cycles. Based on this points, the present work can be considered as a valuable complementary study in the field of cascade oxidation/Knoevenagel condensation. Furthermore, this supramolecular catalyst is a successful example of the combination of chemo- and bio-driven materials catalysis for mimicing biocatalysis and sustainable and one pot multistep synthesis.

Received: 19 August 2019; Accepted: 4 November 2019;

Published online: 28 November 2019

References

1. Yun, G. *et al.* Highly Stable, Water-Dispersible Metal-Nanoparticle-Decorated Polymer Nanocapsules and Their Catalytic Applications. *Angewandte Chemie International Edition* **53**, 6414–6418 (2014).
2. Kelly, K. L., Coronado, E., Zhao, L. L. & Schatz, G. C. The Optical Properties of Metal Nanoparticles: The Influence of Size, Shape, and Dielectric Environment. *The Journal of Physical Chemistry B* **107**, 668–677, <https://doi.org/10.1021/jp026731y> (2003).
3. Wu, N. Plasmonic metal–semiconductor photocatalysts and photoelectrochemical cells: a review. *Nanoscale* **10**, 2679–2696 (2018).
4. Stepanov, A. Optical properties of metal nanoparticles synthesized in a polymer by ion implantation: a review. *Technical Physics* **49**, 143–153 (2004).
5. Efremova, M. V. *et al.* Magnetite-Gold nano hybrids as ideal all-in-one platforms for theranostics. *Scientific Reports* **8**, 11295, <https://doi.org/10.1038/s41598-018-29618-w> (2018).
6. Kwak, N. W. *et al.* In situ synthesis of supported metal nanocatalysts through heterogeneous doping. *Nature Communications* **9**, 4829 (2018).
7. Nisar, A., Lu, Y., Zhuang, J. & Wang, X. Polyoxometalate Nanocone Nanoreactors: Magnetic Manipulation and Enhanced Catalytic Performance. *Angewandte Chemie International Edition* **50**, 3187–3192, <https://doi.org/10.1002/anie.201006155> (2011).
8. Zhang, W., Dynes, J. J., Hu, Y., Jiang, P. & Ma, S. Porous metal-metalloporphyrin gel as catalytic binding pocket for highly efficient synergistic catalysis. *Nature Communications* **10**, 1913 (2019).
9. Segets, D. *et al.* Experimental and theoretical studies of the colloidal stability of nanoparticles – a general interpretation based on stability maps. *ACS Nano* **5**, 4658–4669 (2011).
10. Sehested, J. Sintering of nickel steam-reforming catalysts. *Journal of Catalysis* **217**, 417–426 (2003).
11. Zhang, B., Hu, R., Sun, D., Wu, T. & Li, Y. Fabrication of chitosan/magnetite-graphene oxide composites as a novel bioadsorbent for adsorption and detoxification of Cr (VI) from aqueous solution. *Scientific Reports* **8**, 15397 (2018).
12. Saffarzadeh-Matin, S., Kerton, F. M., Lynam, J. M. & Rayner, C. M. Formation and catalytic activity of Pd nanoparticles on silica in supercritical CO₂. *Green Chemistry* **8**, 965–971 (2006).
13. White, R. J., Luque, R., Budarin, V. L., Clark, J. H. & Macquarrie, D. J. Supported metal nanoparticles on porous materials. Methods and applications. *Chemical Society Reviews* **38**, 481–494 (2009).
14. Kralik, M. & Biffis, A. Catalysis by metal nanoparticles supported on functional organic polymers. *Journal of Molecular Catalysis A: Chemical* **177**, 113–138 (2001).
15. Dekamin, M. G., Kazemi, E., Karimi, Z., Mohammadalipoor, M. & Naimi-Jamal, M. R. Chitosan: An efficient biomacromolecule support for synergistic catalyzing of Hantzsch esters by CuSO₄. *International Journal of Biological Macromolecules* **93**, 767–774, <https://doi.org/10.1016/j.ijbiomac.2016.09.012> (2016).
16. Lang, H., Maldonado, S., Stevenson, K. J. & Chandler, B. D. Synthesis and Characterization of dendrimer templated supported bimetallic Pt–Au nanoparticles. *Journal of the American Chemical Society* **126**, 12949–12956 (2004).
17. Shaban, M., Ashraf, A. M. & Abukhadra, M. R. TiO₂ Nanoribbons/Carbon Nanotubes Composite with Enhanced Photocatalytic Activity; Fabrication, Characterization, and Application. *Scientific Reports* **8**, 781, <https://doi.org/10.1038/s41598-018-19172-w> (2018).
18. Pyun, J. Graphene oxide as catalyst: application of carbon materials beyond nanotechnology. *Angewandte Chemie International Edition* **50**, 46–48 (2011).
19. Li, X. *et al.* Highly active enzyme–metal nano hybrids synthesized in protein–polymer conjugates. *Nature Catalysis*, 1 (2019).
20. Maleki, A., Hajizadeh, Z. & Salehi, P. Mesoporous halloysite nanotubes modified by CuFe₂O₄ spinel ferrite nanoparticles and study of its application as a novel and efficient heterogeneous catalyst in the synthesis of pyrazolopyridine derivatives. *Scientific Reports* **9**, 5552 (2019).
21. Jiang, J. & Yoon, S. A Metalated Porous Porphyrin Polymer with [Co(CO)₄][−] Anion as an Efficient Heterogeneous Catalyst for Ring Expanding Carbonylation. *Scientific Reports* **8**, 13243 (2018).
22. Liu, M. & Li, C. J. Catalytic Fehling's reaction: an efficient aerobic oxidation of aldehyde catalyzed by copper in water. *Angewandte Chemie International Edition* **55**, 10806–10810 (2016).
23. Liu, Q. *et al.* Room-Temperature Copper-Catalyzed Oxidation of Electron-Deficient Arenes and Heteroarenes Using Air. *Angewandte Chemie International Edition* **51**, 4666–4670 (2012).
24. Fan, X., Li, Y., Zhang, X., Qu, G. & Wang, J. An efficient and green preparation of 9-arylacridine-1, 8-dione derivatives. *Heteroatom Chemistry: An International Journal of Main Group Elements* **18**, 786–790 (2007).
25. Sharma, R. K. *et al.* An efficient copper-based magnetic nanocatalyst for the fixation of carbon dioxide at atmospheric pressure. *Scientific Reports* **8**, 1901, <https://doi.org/10.1038/s41598-018-19551-3> (2018).
26. Rudroff, F. *et al.* Opportunities and challenges for combining chemo- and biocatalysis. *Nature Catalysis* **1**, 12–22, <https://doi.org/10.1038/s41929-017-0010-4> (2018).
27. Dumeignil, F. *et al.* From sequential chemoenzymatic synthesis to integrated hybrid catalysis: taking the best of both worlds to open up the scope of possibilities for a sustainable future. *Catalysis Science & Technology* **8**, 5708–5734, <https://doi.org/10.1039/C8CY01190G> (2018).
28. Denard, C. A., Hartwig, J. F. & Zhao, H. Multistep One-Pot Reactions Combining Biocatalysts and Chemical Catalysts for Asymmetric Synthesis. *ACS Catalysis* **3**, 2856–2864, <https://doi.org/10.1021/cs400633a> (2013).
29. Bruggink, A., Schoevaart, R. & Kieboom, T. Concepts of Nature in Organic Synthesis: Cascade Catalysis and Multistep Conversions in Concert. *Organic Process Research & Development* **7**, 622–640, <https://doi.org/10.1021/op0340311> (2003).
30. Meeuwissen, J. & Reek, J. N. H. Supramolecular catalysis beyond enzyme mimics. *Nature Chemistry* **2**, 615, <https://doi.org/10.1038/nchem.744> (2010).

31. Muschiol, J. *et al.* Cascade catalysis – strategies and challenges en route to preparative synthetic biology. *Chemical Communications* **51**, 5798–5811, <https://doi.org/10.1039/C4CC08752F> (2015).
32. Wang, Y., Ren, H. & Zhao, H. Expanding the boundary of biocatalysis: design and optimization of *in vitro* tandem catalytic reactions for biochemical production. *Critical Reviews in Biochemistry and Molecular Biology* **53**, 115–129, <https://doi.org/10.1080/10409238.2018.1431201> (2018).
33. Broadwater, S. J., Roth, S. L., Price, K. E., Kobašlija, M. & McQuade, D. T. One-pot multi-step synthesis: a challenge spawning innovation. *Organic & Biomolecular Chemistry* **3**, 2899–2906, <https://doi.org/10.1039/B506621M> (2005).
34. Yang, Q., Zhang, H.-Y., Wang, L., Zhang, Y. & Zhao, J. Ru/UiO-66 Catalyst for the Reduction of Nitroarenes and Tandem Reaction of Alcohol Oxidation/Knoevenagel Condensation. *ACS Omega* **3**, 4199–4212 (2018).
35. Wang, H., Wang, C., Yang, Y., Zhao, M. & Wang, Y. H₃PW₁₂O₄₀/mpg-C₃N₄ as an efficient and reusable bifunctional catalyst in one-pot oxidation–Knoevenagel condensation tandem reaction. *Catalysis Science & Technology* **7**, 405–417 (2017).
36. Hayashi, Y. Pot economy and one-pot synthesis. *Chemical Science* **7**, 866–880, <https://doi.org/10.1039/C5SC02913A> (2016).
37. Garrabou, X., Wicky, B. I. & Hilvert, D. Fast Knoevenagel condensations catalyzed by an artificial Schiff-base-forming enzyme. *Journal of the American Chemical Society* **138**, 6972–6974 (2016).
38. Bigi, F. & Quarantelli, C. The Knoevenagel Condensation in Water. *Current Organic Synthesis* **9**, 31–39 (2012).
39. Forbes, D. C., Law, A. M. & Morrison, D. W. The Knoevenagel reaction: analysis and recycling of the ionic liquid medium. *Tetrahedron Letters* **47**, 1699–1703 (2006).
40. Dess, D. B. & Martin, J. A useful 12-I-5 triacetoxyperiodinane (the Dess–Martin periodinane) for the selective oxidation of primary or secondary alcohols and a variety of related 12-I-5 species. *Journal of the American Chemical Society* **113**, 7277–7287 (1991).
41. Bi, S. *et al.* Two-dimensional semiconducting covalent organic frameworks via condensation at arylmethyl carbon atoms. *Nature Communications* **10**, 2467 (2019).
42. Dekamin, M. G., Eslami, M. & Maleki, A. Potassium phthalimide-N-oxyl: a novel, efficient, and simple organocatalyst for the one-pot three-component synthesis of various 2-amino-4H-chromene derivatives in water. *Tetrahedron* **69**, 1074–1085, <https://doi.org/10.1016/j.tet.2012.11.068> (2013).
43. Wang, D., Li, Z. & Bi-functional, N. H. 2-MIL-101 (Fe) for one-pot tandem photo-oxidation/Knoevenagel condensation between aromatic alcohols and active methylene compounds. *Catalysis Science & Technology* **5**, 1623–1628 (2015).
44. Qi, Y. *et al.* Design and Synthesis of an Au@ MIL-53 (NH₂) Catalyst for a One-Pot Aerobic Oxidation/Knoevenagel Condensation Reaction. *European Journal of Inorganic Chemistry* **2015**, 5099–5105 (2015).
45. Zhou, W. *et al.* Bifunctional NiGa Layered Double Hydroxide for the Aerobic Oxidation/Condensation Tandem Reaction between Aromatic Alcohols and Active Methylene Compounds. *Asian Journal of Organic Chemistry* **6**, 1536–1541 (2017).
46. Cui, Y., Lee, Y. H. & Yang, J. W. Impact of carboxyl groups in graphene oxide on chemoselective alcohol oxidation with ultra-low carbocatalyst loading. *Scientific Reports* **7**, 3146 (2017).
47. Dekamin, M. G. & Eslami, M. Highly efficient organocatalytic synthesis of diverse and densely functionalized 2-amino-3-cyano-4H-pyrans under mechanochemical ball milling. *Green Chemistry* **16**, 4914–4921, <https://doi.org/10.1039/c4gc00411f> (2014).
48. Shaabani, A. & Lee, D. G. Solvent free permanganate oxidations. *Tetrahedron Letters* **42**, 5833–5836 (2001).
49. Scott, S. L., Bakac, A. & Espenson, J. H. Oxidation of alcohols, aldehydes, and carboxylates by the aquachromium (IV) ion. *Journal of the American Chemical Society* **114**, 4205–4213 (1992).
50. Guibal, E. Heterogeneous catalysis on chitosan-based materials: a review. *Progress in Polymer Science* **30**, 71–109 (2005).
51. Alirezvani, Z., Dekamin, M. G., Davoodi, F. & Valiey, E. Melamine-Functionalized Chitosan: A New Bio-Based Reusable Bifunctional Organocatalyst for the Synthesis of Cyanocinnamionitrile Intermediates and Densely Functionalized Nicotinonitrile Derivatives. *ChemistrySelect* **3**, 10450–10463 (2018).
52. Valiey, E., Dekamin, M. G. & Alirezvani, Z. Melamine-modified chitosan materials: An efficient and recyclable bifunctional organocatalyst for green synthesis of densely functionalized bioactive dihydropyrano [2, 3-c] pyrazole and benzylpyrazolyl coumarin derivatives. *International Journal of Biological Macromolecules* **129**, 407–421 (2019).
53. Ishani, M., Dekamin, M. G. & Alirezvani, Z. Superparamagnetic silica core-shell hybrid attached to graphene oxide as a promising recoverable catalyst for expeditious synthesis of TMS-protected cyanohydrins. *Journal of Colloid and Interface Science* **521**, 232–241 (2018).
54. Dekamin, M. G., Mehdipoor, F. & Yaghoubi, A. 1,3,5-Tris (2-hydroxyethyl) isocyanurate functionalized graphene oxide: a novel and efficient nanocatalyst for the one-pot synthesis of 3,4-dihydropyrimidin-2 (1H)-ones. *New Journal of Chemistry* **41**, 6893–6901 (2017).
55. Rahimi, R., Ghoreishi, S. Z. & Dekamin, M. G. Immobilized metalloporphyrins on 3-aminopropyl-functionalized silica support as heterogeneous catalysts for selective oxidation of primary and secondary alcohols. *Monatshfte für Chemie - Chemical Monthly* **143**, 1031–1038, <https://doi.org/10.1007/s00706-011-0684-2> (2012).
56. Yaghoubi, A., Dekamin, M. G., Arefi, E. & Karimi, B. Propylsulfonic acid-anchored isocyanurate-based periodic mesoporous organosilica (PMO-ICS-Pr-SO₃H): A new and highly efficient recoverable nanoporous catalyst for the one-pot synthesis of bis(indolyl)methane derivatives. *Journal of Colloid and Interface Science* **505**, 956–963, <https://doi.org/10.1016/j.jcis.2017.06.055> (2017).
57. Tian, F., Liu, Y., Hu, K. & Zhao, B. Study of the depolymerization behavior of chitosan by hydrogen peroxide. *Carbohydrate Polymers* **57**, 31–37, <https://doi.org/10.1016/j.carbpol.2004.03.016> (2004).
58. Dalcanale, E. & Montanari, F. Selective oxidation of aldehydes to carboxylic acids with sodium chlorite-hydrogen peroxide. *The Journal of Organic Chemistry* **51**, 567–569, <https://doi.org/10.1021/jo00354a037> (1986).
59. Kita, E. & Uścińska, G. A kinetic study of the oxidation of 2-pyridinmethanol, 2-pyridinocarboxaldehyde and 2,6-pyridinedimethanol by chromium(VI) in acidic aqueous media. *Transition Metal Chemistry* **28**, 373–380, <https://doi.org/10.1023/A:1023625426692> (2003).
60. Rahman, T., Borah, G. & Gogoi, P. K. Hybrid composite of CuO with g-C₃N₄ as a photoactive catalyst: an efficient approach for the oxidation of alcohols. *Journal of Chemical Sciences* **131**, 4, <https://doi.org/10.1007/s12039-018-1581-6> (2019).
61. Gogoi, N., Begum, T., Dutta, S., Bora, U. & Gogoi, P. K. Rice husk derived nanosilica supported Cu (II) complex: an efficient heterogeneous catalyst for oxidation of alcohols using TBHP. *RSC Advances* **5**, 95344–95352 (2015).
62. Dekamin, M. G., Azimoshan, M. & Ramezani, L. Chitosan: a highly efficient renewable and recoverable bio-polymer catalyst for the expeditious synthesis of [small alpha]-amino nitriles and imines under mild conditions. *Green Chemistry* **15**, 811–820, <https://doi.org/10.1039/C3GC36901C> (2013).
63. Rosen, B. M. *et al.* The disproportionation of Cu(I)X mediated by ligand and solvent into Cu(0) and Cu(II)X₂ and its implications for SET-LRP. *Journal of Polymer Science Part A: Polymer Chemistry* **47**, 5606–5628, <https://doi.org/10.1002/pola.23690> (2009).
64. Yan, H., Zhang, H.-Y., Wang, L., Zhang, Y. & Zhao, J. Ru (OH) x supported on polyethylenimine modified magnetic nanoparticles coated with silica as catalyst for one-pot tandem aerobic oxidation/Knoevenagel condensation of alcohols and active methylene compounds. *Reaction Kinetics, Mechanisms and Catalysis* **125**, 789–806 (2018).

Acknowledgements

We are grateful for the financial support from The Research Council of Iran University of Science and Technology (IUST), Tehran, Iran (Grant No. 160/18517). We would also like to acknowledge support of The Iran Nanotechnology Initiative Council (INIC).

Author contributions

(1) Zahra Alirezvani worked on the topic as her Ph.D Thesis and prepared the initial draft of the manuscript. (2) Dr. Mohammad G. Dekamin is supervisor of Miss Alirezvani and Mr. Valiey as his Ph.D. students. Also, he edited and revised the manuscript completely. (3) Ehsan Valiey worked closely with Miss Alirezvani for doing experimental section.

Competing interests

The authors declare no competing interests.

Additional information

Supplementary information is available for this paper at <https://doi.org/10.1038/s41598-019-53765-3>.

Correspondence and requests for materials should be addressed to M.G.D.

Reprints and permissions information is available at www.nature.com/reprints.

Publisher's note Springer Nature remains neutral with regard to jurisdictional claims in published maps and institutional affiliations.



Open Access This article is licensed under a Creative Commons Attribution 4.0 International License, which permits use, sharing, adaptation, distribution and reproduction in any medium or format, as long as you give appropriate credit to the original author(s) and the source, provide a link to the Creative Commons license, and indicate if changes were made. The images or other third party material in this article are included in the article's Creative Commons license, unless indicated otherwise in a credit line to the material. If material is not included in the article's Creative Commons license and your intended use is not permitted by statutory regulation or exceeds the permitted use, you will need to obtain permission directly from the copyright holder. To view a copy of this license, visit <http://creativecommons.org/licenses/by/4.0/>.

© The Author(s) 2019